Korean J. Chem. Eng., 37(10), 1761-1772 (2020)
DOI: 10.1007/s11814-020-0584-4

pISSN: 0256-1115
eISSN: 1975-7220

Synthesis of Chitosan/Maleate-Alumoxane nanocomposite membranes for adsorption of anionic dye

Pegah Amiri*, Jamshid Behin*,†, Laleh Rajabi, and Meisam Ansari***

*Advanced Chemical Engineering Research Center, Faculty of Petroleum and Chemical Engineering, Razi University, Kermanshah, Iran
**Polymer Research Center, Faculty of Petroleum and Chemical Engineering, Razi University, Kermanshah, Iran
(*Received 3 December 2019 • Revised 14 March 2020 • Accepted 16 May 2020*)

Abstract−Chitosan/Mal-A nanocomposite membranes were synthesized and used for adsorption of Reactive Yellow 84 (RY 84) from aqueous solution. The membranes were prepared by solution-casting method with 2 wt% Chitosan (Cs) and various ratios of Mal-A (0.3-0.9 wt%). FTIR and SEM analyses were used to characterize the Cs-based membrane. The results showed that a dense-thin-face layer associated with an open-structure layer was formed in the composite membrane containing 0.5 wt% Mal-A. Membrane performance was investigated as dye removal and permeate flux. The significant effects of the operating variables including pH, initial concentration of dye, and Cs/Mal-A dose, were evaluated on RY removal efficiency using response surface methodology (RSM). The results obtained from the experimental data were presented with the quadratic regression model. The adsorption kinetics and equilibrium isotherm were well described by the pseudo-second order and the Langmuir model, respectively. Adding Mal-A nanoparticles to the Cs matrix (0.5 wt%) improved liquid permeability by 21% compared with the Cs membrane, while dye removal efficiency for both membranes remained approximately 100% at acidic pH and under a trans-membrane pressure of 3 bar. The protonation of the amine groups in CS/Mal-A results in a positive charge on the membrane surface which causes a complete removal of the anionic dye. The permeability improvement of ~57.2% for the composite membrane was achieved at a pressure difference of 5 bar, which corresponded to an efficiency reduction of 10%.

Keywords: Nanocomposite Membrane, Chitosan, Maleate-Alumoxane, Reactive Yellow 84, Adsorption

INTRODUCTION

The large number of synthetic dyes commonly used in textile industry generate hazardous effluent into the environment. The reactive dyes are the main group among the textile azo dyes due to their bright colors, high photolytic stability, and superior fastness properties. Besides the unfavorable colors of textile effluents, certain dyes can degrade to produce toxic/carcinogenic products [1], and their deletion becomes a significant environmental concern [2]. Nowadays, several removal methods have been used including adsorption [3], coagulation [4], membrane separation/filtration [5], flocculation [6], microbiological decomposition [7], fungus bio-sorption [8], and photo-catalytic treatment [9]. Among them, adsorption is one of the most effective because of ease of use and operating cost [10]. Chitosan biopolymer [11] has gained more attention compared to other commercial adsorbents such as activated carbon [12] and various zeolitic materials [13] due to its specific characteristics such as high molecular structure, high adsorption capacity, abundance and relatively low price [14].

Although the adsorption potential of different forms of chitosan has been explored for the removal of dye from aqueous waste [15, 16], the loss of its sorption capacity under acidic conditions is already a drawback [17]. Hence, micro/nano-composite powder and membrane adsorbent based on chitosan (Cs) were found to be the promising forms [18,19]. Improvement of mechanical properties and efficiency of Cs for dye removal were considered as the main objectives of the manufacture of such composites [20]. A Cs/ZnO nanocomposite powder was successfully used to remove two types of textile dyes from aqueous effluents [21]. Recently, a porous Cs/Hydroxyapatite membrane was synthesized to test the dynamic removal of textile dye. The optimum removal condition was obtained using the membrane containing 30% hydroxyapatite in acidic solution [22]. Because of its useful synergic properties, nanocomposites can increase liquid flux, dye removal efficiency and strength of polymer base membrane [23].

The blending of nanocomposite membranes with inorganic fillers will combine the benefits of the polymer matrix with those of the filler material [24]. Cs/dialdehyde micro-fibrillated cellulose composite membrane was used to remove an anionic dye and a high adsorption capacity (152.5 mg/g) was obtained [25]. Carboxylate-alumoxanes were used among the inorganic fillers to cover polystyrene capsules and form a hierarchical nano-filtration membrane [26]. These are alumina nanostructures where the surface is coated with covalently bound carboxylate groups via the reaction between boehmite (g-AlOOH) and carboxylic acid (HO_2CR). In fact, the alumoxane's properties can be managed by selecting organic molecules. Adding carboxylate-alumoxane with appropriate functional groups to a polymer membrane can enhance the physicochemical characteristics of the polymeric base membrane.

The aim of this research was to investigate the effect of adding

†To whom correspondence should be addressed.
E-mail: Behin@razi.ac.ir

Maleate-Alumoxane (Mal-A) nanoparticles to Cs by studying the physical property, dye adsorption capacity, and permeate flux of the synthesized membrane. Reactive Yellow 84 (RY84) was chosen as a model contaminant because it has been commonly used commercially but is hardly removed with conventional processes due to aromatic rings in its structure [27]. The optimal Mal-A content was found in the Cs/Mal-A membrane and the synthesized nanocomposite membrane was used for further adsorption experiments. Response surface methodology (RSM) was used to assess the impact of operating variables on removal efficiency [28]. A dead-end filtration set-up, similar to the literature [29], was used for the dynamic removal experiments.

EXPERIMENTALS

1. Materials

Aluminum nitrate ($Al(NO_3)_3{\cdot}9H_2O$), sodium hydroxide (NaOH), and maleic anhydride of analytical grade were purchased from Merck (Germany) and used without further purification. Chitosan powder (low molecular weight and 75-85% deacetylated) was supplied by Sigma-Aldrich (Germany). RY 84 dye (chemical formula: $C_{50}H_{24}Cl_2N_{14}Na_{10}O_{30}S_{10}$) was obtained from Boyakh-Saz Company of Tabriz (Iran). All solutions were prepared with deionized water and the other reagents including acetone, maleic acid, fumaric acid, ethanol, 2-hydroxybenzoic acid, 4-aminobenzoic acid were of the analytical grade obtained from Merck (Germany).

2. Boehmite Nanoparticles

The method described in previous study [30] has been used to prepare boehmite nanoparticles. Two solutions were prepared that contain 6.490 g NaOH in 50 mL and 20 g $Al(NO_3)_3{\cdot}9H_2O$ in 30 mL deionized water, respectively. The NaOH solution was then poured into the other solution within 17 min at the rate of 2.94 mL/min with intense agitation. The resulting milky liquid was mixed at a controlled temperature of 25±1 °C for around 3 h in the ultrasonic bath (Bandelin Sonrex Digitec, DT52H type, Germany). To obtain boehmite nanoparticles, the resulting precipitate was filtered, rinsed with deionized water, and put in the oven at a temperature of 220 °C for duration of 4 h.

3. Mal-A Nanoparticles

In a round-bottomed flask of 500 mL in volume, 6 g boehmite and 9.8 g maleic anhydride (equimolar compositions) were blended completely in 200 mL deionized water. The obtained mixture was sonicated for 10 min and then refluxed for 10 h at its normal boiling point. It was then cooled gradually to ambient temperature and centrifuged. The precipitate was carefully rinsed with acetone and deionized water to remove the unreacted maleic acid. The resulting suspension was centrifuged and the precipitate was dried in the oven at 80 °C.

4. Asymmetric Cs/Mal-A Nanocomposite Membrane

A certain amount of Mal-A (0.3, 0.5, and 0.9 wt%) was dissolved in a 1% (v/v) acetic acid solution. The range of Mal-A dose was chosen to achieve a significant improvement in dye adsorption, according to the preliminary tests. The resulting mixture was bath-sonicated for 10 min to achieve complete dissolution. The chitosan powder (2 wt%) was then added to the solution and incubated at room temperature below the 180 rpm shaking for 24 h. Afterward, the resulting mixture was maintained in a beaker at 50 °C for 48 h without stirring to release the dissolved air. Cross-linking between Cs and Mal-A nanoparticles was considered to be established at low temperature and long resting time. The carboxylate moiety acts as a ligand for vacant coordination sites of surface metal atoms. Despite this, the coordination bond is weak and can be broken or replaced by other ligand molecules by increasing the temperature. The collected solution was then cast on the glass plates using a doctor blade with a thickness of about 150 μm and dried at ambient temperature. To make membrane insoluble in water and also to neutralize the excess acid, it was immersed into 1 M alkaline NaOH solution for ~1 h, then washed exhaustively with deionized water and dried for 24 h at ambient temperature. Plain membrane was also similarly prepared using Cs alone.

The prepared Mal-A and Cs/Mal-A membranes were characterized taking Fourier transform infrared spectroscopy (FTIR, ABB Bomem, MB-104, Canada) and scanning electron microscopy (SEM) images (Philips-X130, Netherland). The thickness and the tensile strength of the synthesized membranes were measured using a micrometer (Guanglu, China) and an UTM4503SLXY-type universal material testing machine (China), respectively. The samples were cut into strips of 70×10×0.1 mm and subjected to tensile testing at a rate of 2 mm/min as per standard GB/T 100.3-2006 (the gauge length was set to 50 mm).

5. Static Adsorption Experiments

The adsorption tests were conducted in a batch mode under the optimum level of investigated variables. The RSM based on Box-Behnken Design (BBD) was used to quantify the impact of operation variables on RY removal efficiency and to find the optimum experimental conditions. The Design-Expert software (version 10) was used for statistical analysis and for evaluating the interaction between the variables. The pH (X_1), the initial concentration of dye (X_2), and the Cs/Mal-A dose (X_3) were considered as the independent variables and the RY removal efficiency (Y) was considered as the dependent (response) variable. The RY removal efficiency in batch mode was obtained using the following equation:

$$Y(\%) = \left(1 - \frac{C_e}{C_o}\right) \times 100 \quad (1)$$

where, C_o and C_e are the initial and equilibrium RY concentrations in aqueous solution (mg/L), respectively. The concentration of the dye was measured at wavelength of 339 nm using a UV-Vis spectrophotometer (cecil-7250, UK). The ranges of coded and un-coded levels of the selected variables are listed in Table 1. A constant equilibrium period of 240 min was considered in all experimental runs.

Experimental data were correlated using a second-order polynomial model as follows:

Table 1. Coded and un-coded levels of the experimental variables

Independent variable	Unit	Symbol	Coded level		
			−1	0	1
pH	-	X_1	4	7	10
Dye initial concentration	mg/L	X_2	20	50	80
Cs/Mal-A dose	g/L	X_3	0.2	0.8	1.4

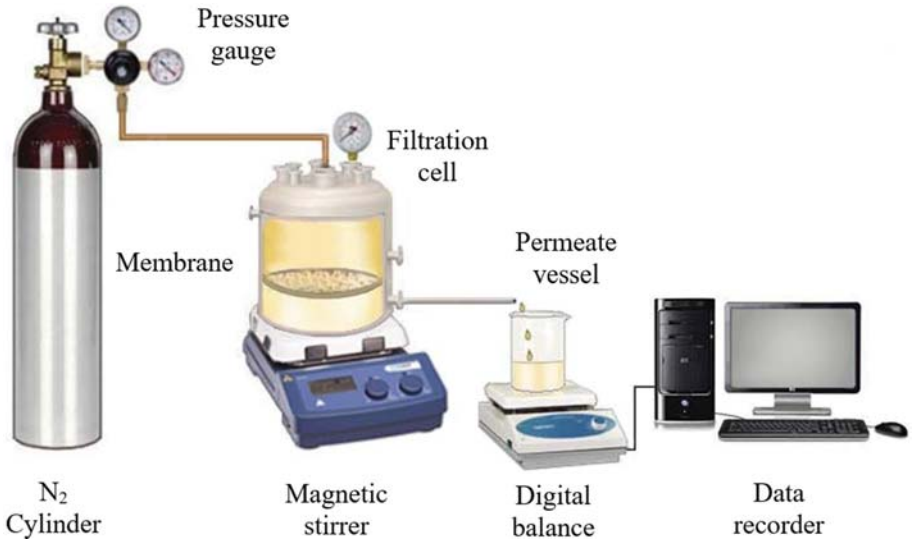

Fig. 1. A schematic of the dead-end filtration set-up.

$$Y\,(\%) = b_o + \sum_{i=1}^{n} b_i X_i + \sum_{i=1}^{n} b_{ii} X_i^2 + \sum_{i=1}^{n-1} \sum_{j=i+1}^{n} b_{ij} X_i X_j + e \quad (2)$$

where Y is the response factor, b_o is the constant of equation, b_i, b_{ii}, b_{ij} are the coefficients for the linear, quadratic and interaction effect, X_i and X_j are the coded values of the variables, n and e are the number of variables and the random error, respectively. The fitting quality of the model equation was expressed by the coefficient of determination, R^2.

The quantity of adsorbed RY at equilibrium conditions, adsorption capacity (mg/g), was determined as follows:

$$q_e = \frac{(C_o - C_e)V}{M} \quad (3)$$

where, C_o and C_e are the initial and equilibrium concentrations of RY (mg/L), respectively, V and M are the volume of solution (L) and the mass of adsorbent (g), respectively.

6. Dynamic Adsorption Experiments

Dynamic dye removal experimental runs were performed in a dead-end filtration cell as schematically illustrated in Fig. 1. The cell volume was 200 mL with a membrane surface area of 12.56 cm^2. A compressed nitrogen cylinder was used to supply pressure in the cell which was mounted on a 300 rpm magnetic stirrer. Permeate was collected and its weight was continuously measured using a digital balance during the experimental period. The permeate flux was determined based on the changes in the accumulative mass of permeate as a function of time. The liquid flux and RY removal efficiency of selected membranes were defined under the trans-membrane pressure ranging from 3 to 5 bar and temperature 25 °C.

The permeate flux (kg/m^2h) was calculated from the following equation:

$$J = \frac{M}{A \cdot \Delta t} \quad (4)$$

where, M, A, and Δt are the mass of permeated liquid (kg), the membrane surface area (m^2), and the permeation time (h), respectively.

The dynamic RY removal efficiency, η_d, was obtained with the following equation:

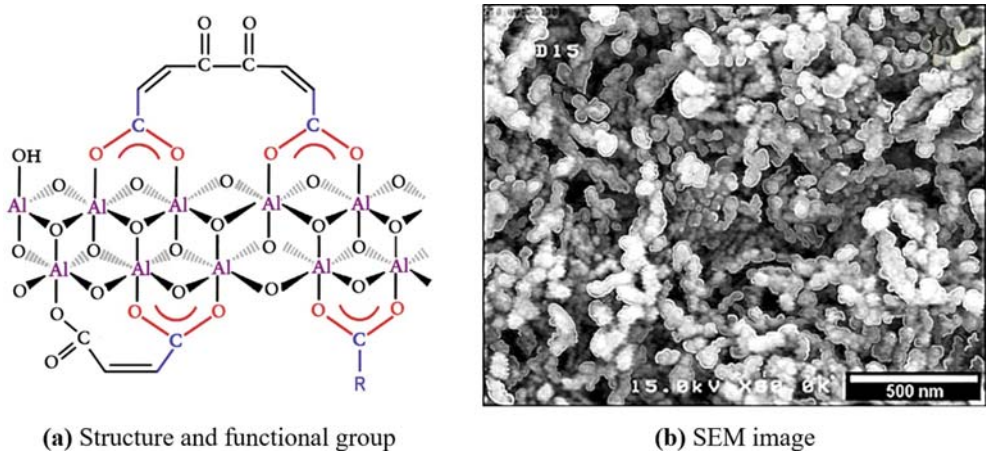

(a) Structure and functional group **(b)** SEM image

Fig. 2. Synthesized Mal-A nanoparticles.

$$\eta_d(\%) = \left(1 - \frac{C_p}{C_f}\right) \times 100 \quad (5)$$

where, C_f and C_p are the concentrations of RY (mg/L) in feed and permeate, respectively.

RESULTS AND DISCUSSION

1. Characterization of Mal-A Nanoparticles

Fig. 2(a) exhibits the structure of Mal-A nanoparticles identical to the original boehmite. However, their surface reacted partly with carboxylate groups; consequently, some OH groups, attached on the surface, remained unreacted due to space congestion. Among possible coordination states of carboxylate ligands and aluminum ions on the boehmite surface, bonding to two Al atoms appears to be the most stable. Therefore, carboxylates are more likely to bind to the boehmite surface through this state. The reason for this stability is the formation of six-membered loops that are stabilized by resonance. The reaction of carboxylic group with the double-layered aluminum oxide hydroxide (boehmite) may be ideally considered as an exchange reaction where the carboxylate ion replaces some of the hydroxyl groups on the oxide double layer surface and bridges other aluminum sites. Fig. 2(b) displays the SEM image of Mal-A, where the nanoparticles were observed with an average diameter of ~50 nm and the dominant morphology of the nanoparticles was filamentous granular. This is caused by the aggregation and bonding of nanoparticles together.

2. Optimal Content of Mal-A in Composite Membrane

Dye removal efficiency was determined using the Cs/Mal-A composite membrane at different Mal-A weight ratios (0.3 to 0.9 wt%) and compared with the Cs membrane alone. The adsorption experiments were performed at the mean level of independent variables. As shown in Fig. 3, it is evident that the removal efficiency increased with incorporation of Mal-A in the membrane matrix. The lowest and the highest adsorption efficiency was achieved with Cs and Cs/Mal-A membrane containing 0.9 wt% of Mal-A, respectively. Increasing the Mal-A content by more than 0.9 wt% resulted in an insignificant-slight increase in removal efficiency. The high blending ratio led to an agglomeration of the active sites within the pores of the Cs/Mal-A membrane, which resulted in a reduction of surface functional groups of the Cs membrane. The removal efficiency was relatively close together for the Mal-A content between 0.5 and 0.9 wt%. Moreover, according to preliminary analyses, a tensile strength of 27.4, 30.8 and 31.3 MPa was obtained for Cs, Cs/Mal-A (0.5 wt%) and Cs/Mal-A (0.9 wt%) flat sheet membranes, respectively. A slight increase (approximately 1.6%) was observed in tensile strength with 0.4% extra content of Mal-A. Considered overall, 0.5 wt% Mal-A was chosen as the optimal dose for further experiments because it saved the consumption of Mal-A nanoparticles (economically) and preserved the least mechanical characterization aspect of the synthesized-composite membrane.

3. Characterization of Cs and Cs/Mal-A Composite Membrane

Fig. 4 illustrates FTIR spectra of boehmite, Mal-A, Cs, and Cs/Mal-A samples. Two intense bands appearing in the FTIR spectrum of boehmite at 3,076 and 3,288 cm^{-1} correspond to the stretch frequency of OH groups. The more profound the bands, the more will be the structural uniformity of the boehmite. The frequencies of 1,068 and 1,153 cm^{-1} are attributed to the symmetrical bending vibrations of hydrogen bands of OH··OH. The frequencies of 732, 607, and 460 cm^{-1} belong to Al-O vibration modes [30]. Other peaks represented in the FTIR spectrum of boehmite either belong to nitrate anion or combined diversity, and overtones. However, the FTIR spectrum of Mal-A shows the prominent peaks of boehmite, indicating the amount of unreacted OH groups of boehmite on the surface of Mal-A. Moreover, the two broad and prominent peaks at 1,560 and 1,450 cm^{-1} approve the creation of carboxylate links on nanoparticles surface on reacting with maleic anhydride.

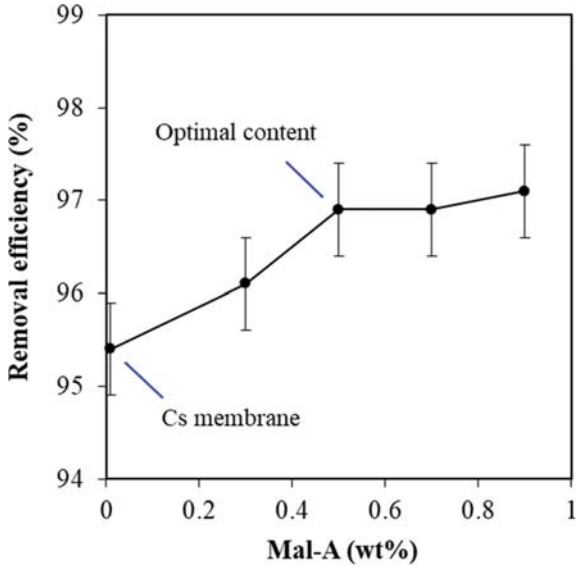

Fig. 3. Dye removal efficiency of synthesized membrane at the mean level of variables (initial concentration of RY: 50 mg/L; Cs/Mal-A dosage: 0.8 g/L; pH: 7 and adsorption period: 240 min).

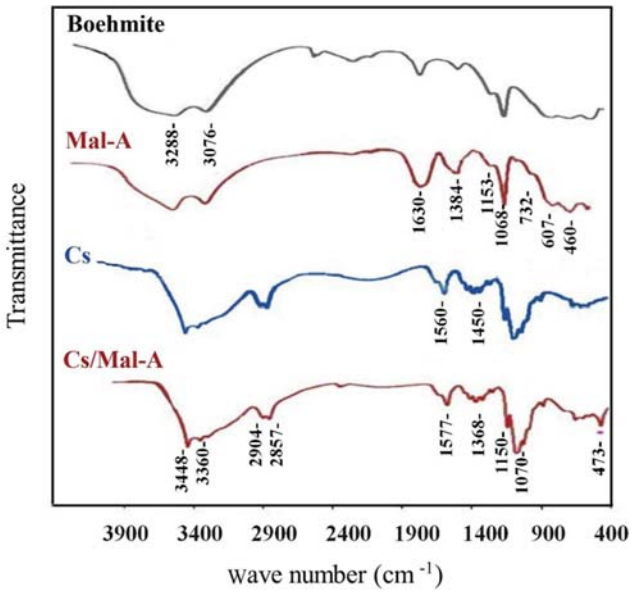

Fig. 4. FTIR spectra of the samples: Boehmite, Mal-A powder, Cs and Cs/Mal-A membranes.

Furthermore, the overspread broad peak at 1,600 cm^{-1} belongs to the stretching vibration of C=C in the maleate structure. The peaks of the Cs/Mal-A membrane display a higher absorption than that of the Cs membrane due to the addition of Mal-A nanoparticles to the chitosan. However, they were similarly shifted by only a few cm^{-1} after complexation with nanoparticles. Observed changes in the absorption bands of the amino groups, carboxyl groups, and amide bonds can be attributed to an ionic interaction between the carbonyl group of nanoparticles and the amino group of chitosan. The peak absorbance of amino groups of chitosan at 1,150 cm^{-1} was also present after complexation and absent in Mal-A nanoparticles. These findings indicate an effective polymer interaction and tend to be in accordance with the stoichiometric ratios between them suggesting a prevalence of Mal-A in the final blend. Nevertheless, the peak at 473 corresponds to the vibrations of Al-O-Al bonds oxide of nanoparticles. Other peaks can be observed as overlapping.

Fig. 5(a) and (b) displays the SEM images of the surface Cs and Cs/Mal-A membranes (Cs: 2 wt%, Mal-A: 0.5 wt%), respectively. A fairly rough surface was observed in Cs morphology (Fig. 5(a)). The sponge-like surface of Cs membrane showed a mechanically poor structure. The distribution of organic-inorganic Mal-A nanoparticles within the polymeric structure can influence the physical characteristics of the composite membrane. A homogeneous dense structure with a smooth surface was formed by the addition of the Mal-A nanoparticles to Cs (Fig. 5(b)) indicating a mechanically strong membrane. The structure of the synthesized membrane was likewise comparable with that of the Cs membranes/composite-membranes previously synthesized and reported in the literature [31-33]. The introduction of nanoparticles to the Cs membrane resulted in the creation of a nano-contexture in the membrane structure; more sites became available to increase the membrane permeate flux.

Fig. 5(c) and (d) demonstrates the cross-section SEM image of the synthesized membranes. The thickness of dry membranes was in range of 4-10 μm. Cs membrane (Fig. 5(c)) exposed a uniform dense matrix; however, the presence of Mal-A nanoparticles in the Cs membrane resulted in the formation of the pathways and nano-scale channels as shown (green lines) in the cross-section of the composite membrane (Fig. 5(d)). The Mal-A nanoparticles established a specific interaction with the Cs matrix, which resulted in such structure being developed. A relatively porous interconnected structure of Cs/Mal-A membrane made it suitable for penetration of the dye and liquid permeation through the membrane; however, a dense-thin layer was observed on the surface. Anisotropic (asymmetric) membrane consisted of relatively dense-thin facial layers backed by an open, much thicker porous substructure. The dense layers of the surface were extremely thin and highly cross-linked. The separation properties have been controlled exclusively by the

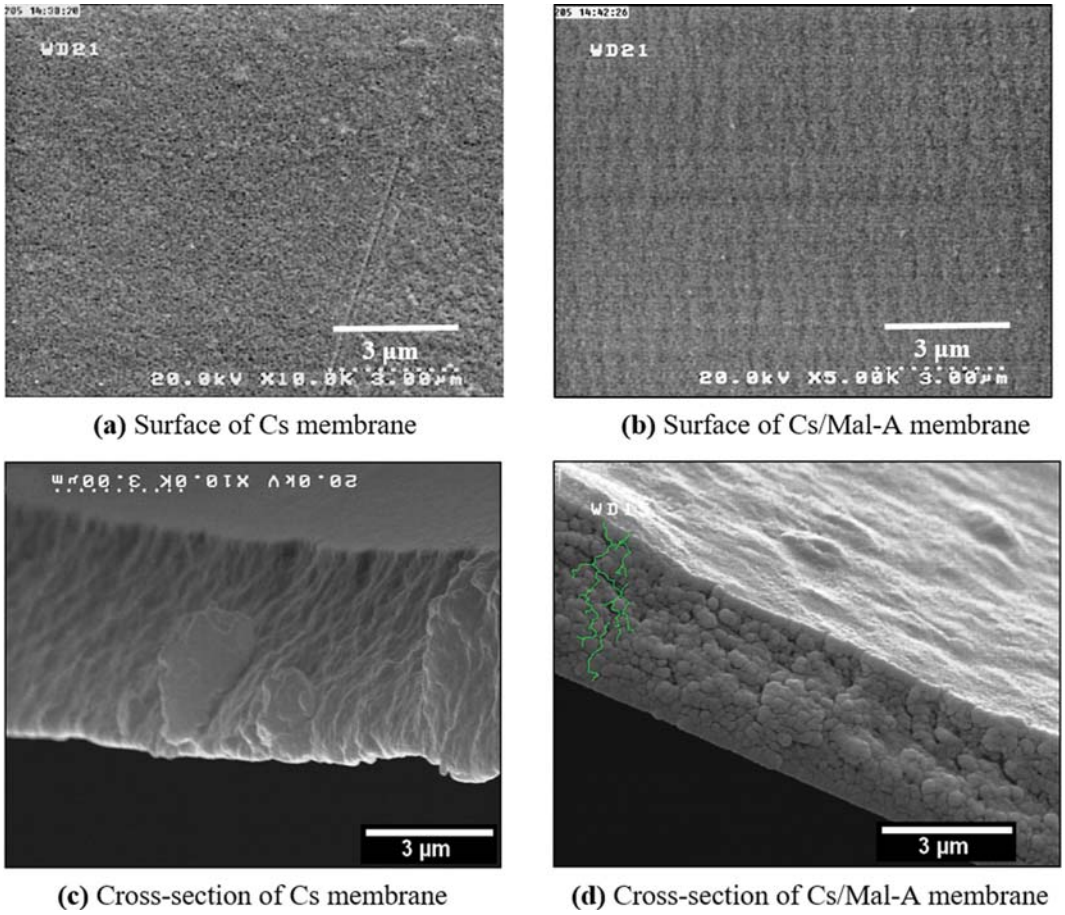

Fig. 5. SEM image of synthesized membranes.

Table 2. Range of the investigated variables in the BBD design of experiment

Run no.	Coded variable			RY removal efficiency (%)	
	X_1	X_2	X_3	Experimental (Y)	Predicted (Y)
1	0	−1	+1	98.18	>100.00
2	−1	0	+1	82.27	83.47
3	0	+1	+1	55.78	57.45
4	+1	0	−1	27.75	30.55
5	−1	+1	0	26.71	30.13
6	+1	+1	0	36.87	30.47
7	−1	0	−1	43.50	50.69
8	+1	0	+1	75.77	72.57
9	0	0	0	41.25	42.58
10	0	0	0	36.50	42.58
11	0	+1	−1	16.56	15.31
12	+1	−1	0	64.75	65.33
13	0	−1	−1	68.43	70.77
14	−1	−1	0	86.31	96.71
15	0	0	0	44.01	42.58

surface layers. This composite membrane has the advantage of determining the membrane selectivity and flux. The pore increment in the composite membrane structure provided the mechanical strength and allowed the manufacture of a thin membrane (4-10 μm) with higher permeate flux. Moreover, the solution containing RY can be distributed across the polymeric matrix and access the adsorption sites without the osmotic pressure gradient.

4. Statistical Design and Optimization

The complete design matrix associated with the response values (RY removal efficiency) according to experiments is outlined in Table 2. Fifteen experimental runs were determined by the software and the experiments were repeated in the central point three times to be more precise.

Analysis of variance (ANOVA) justified the adequacy of the model accurately, and a quadratic model was chosen as the software selection for the RY removal efficiency. The polynomial equation of second order was well adapted to the removal efficiency (Y) experimental results and was expressed in coded variables as:

$$Y\,(\%)=42.58-7.76X_1-25.36X_2+18.70X_3+5.33X_1^2+7.75X_2^2 +11.41X_3^2+7.93X_1X_2+2.31X_1X_3+2.37X_2X_3 \quad (6)$$

Table 3 summarizes the findings of the ANOVA results for the aforementioned model. It is essential to describe the importance and adequacy of the developed model.

Model terms were examined with the p-value and a value less than 0.05 was regarded as significant [34]. The significant model terms were X_1, X_2, X_3, X_2^2, X_3^2, X_1X_2, and the interaction of the other variables including X_1^2, X_1X_3, X_2X_3 on the response can be ignored. The first-order main effects, i.e., the initial concentration of dye (X_2) and adsorbent dose (X_3) have nonlinear impact on removal efficiency, while it varied almost linearly with liquid acidity (X_1). This may be due the nonlinearity of equilibrium behavior for higher levels of X_2 and lower levels of X_3 (deviation from Henry's law). The binary interaction term shows how the response changes when two variables change accordingly. As regards interactive terms, X_1X_2 has a synergistic effect on the removal efficiency and is more important than X_1X_3 and X_2X_3. Increasing the initial concentration of dye (X_2) and reducing the adsorbent dose (X_3) separately contributes to the rise in the driving force for mass transfer from bulk of liquid to the solid surface. Their effects are combined with superposition theory. The pH (X_1) and the adsorbent dose (X_3) are equally interactive. Increasing initial concentration of dye (X_2) increases adsorption capacity under the equilibrium condition, but it is highly dependent on pH. At acidic pH, the protons on the solid surface attract negative charged group of dye and help increase the mass transfer and shift the equilibrium curve to the higher adsorption capacity. Therefore, the interaction between these two factors can be more effective than any change in each of these factors alone. This is not the case with the X_1X_3 and X_2X_3 interactions.

The high R^2 value (0.989) for RY removal indicated that 98.94%

Table 3. ANOVA for the quadratic model predicting dyes adsorption efficiency on the Cs/Mal-A composite

Source	Degree of freedom	Sum of squares	Mean squares	F-value	p-Value
Model	9	8,313.41	923.71	51.84	0.0002
X_1	1	245.42	245.42	13.77	0.0138
X_2	1	4,210.25	4,210.25	236.29	<0.0001
X_3	1	2,288.94	2,288.94	128.46	<0.0001
X_1X_2	1	251.50	251.50	14.12	0.0132
X_1X_3	1	21.39	21.39	1.20	0.3232
X_2X_3	1	22.41	22.41	1.26	0.3130
X_1^2	1	104.88	104.88	5.89	0.0597
X_2^2	1	221.59	221.59	12.44	0.0168
X_3^2	1	480.49	480.49	26.97	0.0035
Model error	5	89.09	17.82		
Lack-of-fit	3	60.25	20.08	1.39	0.443
Pure error	2	28.85	14.42		
Total	14	8,402.50			

R^2: 0.9894, R^2_{adj}: 0.9703, Adeq. precision: 24.48

of variations in the responses could be described with the model. The R^2_{adj} value (0.970) advocated a high significance in this model and it was in reasonable agreement with R^2_{pred} (0.878). Besides, the relatively high value of adequate precision (24.48) indicated that this model was appropriate for the process. The lack of fit p-value (0.443) was higher than 0.05, while non-significant lack-of-fit mean that that quadratic model was valid for the sorption RY onto the Cs/Mal-A adsorbent.

The diagnostics analysis was completed by normal probability plots of residuals to judge the model satisfaction. There was a satisfactory agreement between the predicted and experimental removal efficiency values and the residuals followed a normal distribution pattern (Figures not shown) suggesting the model's adequacy.

Fig. 6 reveals the binary interactions of three independent variables on removal efficiency. Such plots display interaction between two variables, whereas other variables are maintained constant at their own fixed-medium level. It is useful to find the interaction impacts of these mutual factors on removal efficiency. Contour plots make it easier to directly explore the effects of experimental variables on responses. Fig. 6(a) illustrates the synergic impact of the initial dye concentration and the pH on removal efficiency. Acidity of medium is one of the most important factors affecting the adsorption of dye onto solid surface. Generally, the removal efficiency increases at low pHs for an anionic dye such as RY [35,36]. For chitosan adsorbent alone, maximum adsorption of RY 84 was observed at the lowest pH because of physical adsorption of anionic dyes, mainly due to protonation of the amine groups of chitosan [17]. The high occupancy of H^+ ions on the Cs/Mal-A surface provides more sites for absorption. The positively charged surface functions can attract the negatively charged sulfonate groups (SO_3^-) present in the reactive diazo dye molecule more easily. The Mal-A nanoparticles and RY dye molecules interact with each other in two ways: i) an alkene double-bond of Mal-A and that of RY dye (type π-π) and ii) an hydrogen type between -OH group of Mal-A and hydrogen of dye molecule. Reduction of pH contributes to protonation of the -OH groups of Mal-A nanoparticles and formation of $-OH_2^+$ groups that increases the electrostatic forces with $-SO_3^-$ groups of dye molecules. Increasing the concentration of dye at a constant pH often decreased the removal efficiency (Fig. 6(a)). As the dye concentration increases, the more repulsive forces will appear among

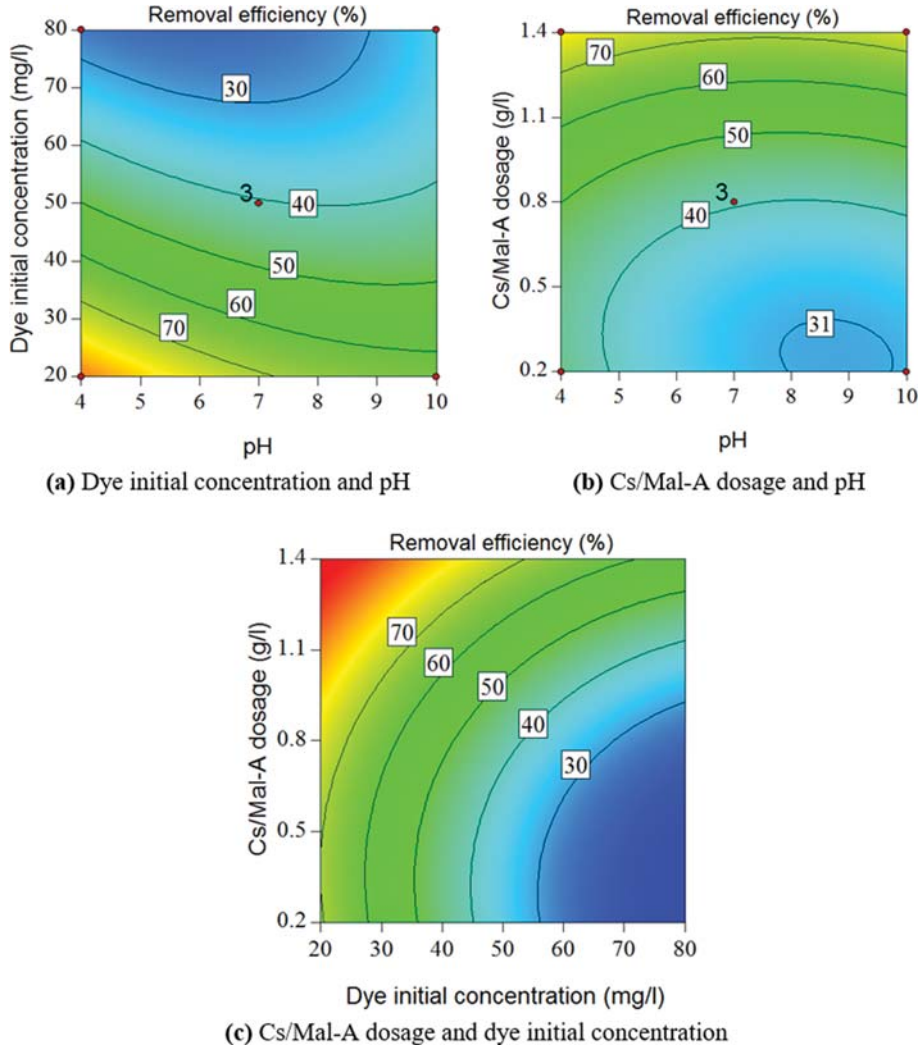

Fig. 6. The binary interaction of independent variables on RY removal efficiency.

the negatively charged groups (SO_3^-) of dye molecules and the equilibrium will shift to counteract the effect of this constraint and increase the adsorption capacity. Therefore, the dye molecules occupied the more active sites in the Cs/Mal-A structure. However, the increasing rate of dye concentration is much higher than that of capacity and the removal efficiency (Eq. (1)) decreases as a consequent.

The effect of the Cs/Mal-A dose and pH on the removal efficiency is demonstrated in Fig. 6(b). The observed trend may be due to the influence of pH on both the surface state of the Cs/Mal-A membrane and the ionization state of the organic molecule of the RY dye. The removal efficiency clearly improved with the dose of Cs/Mal-A at a constant pH. The effect of the Cs/Mal-A dose and the initial concentration of dye on the adsorption efficiency is displayed in Fig. 6(c). The greater adsorbent dosage led to more empty exchange sites on solid surface that pushed the system towards greater adsorption (Le Chatelier's principle). However, as a result the removal efficiency increased at a constant initial concentration of dye.

The goal for variables was set to an exact value, and the decision goals for responses were "maximize" and "within range". The maximum level should be considered for removal efficiency. The optimum value of the main factors for removal efficiency was provided using numerical optimization. Table 4 summarizes the lower and the upper limits of the variables and the response, and the best solution proposed by the software. The removal efficiency result achieved from a verification study confirmed the data predicted from desirability optimization using statistical design.

5. Adsorption Kinetics and Isotherms

The adsorption process was studied for a contact period up to 240 min. The adsorption capacity of RY was reached 15.8 and 24.9 mg/g for Cs and Cs/Mal-A, respectively, in less than 2 h (115 min).

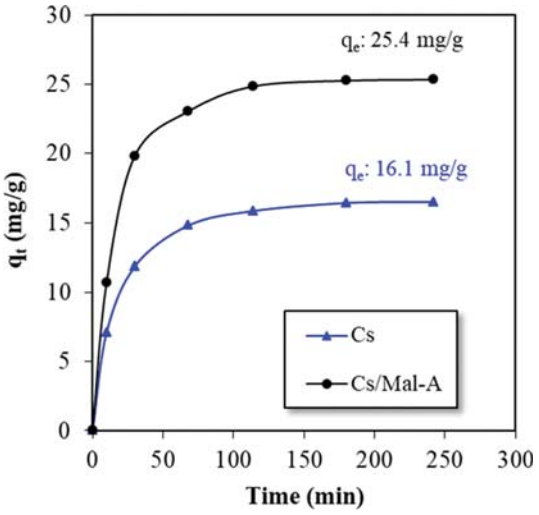

Fig. 7. Adsorption capacity of Cs and Cs/Mal-A composite membrane at the mean level of variables ranges (agitation speed: 180 rpm, temperature: 25 °C).

Then, the rate of adsorption slowed gradually and reached a plateau (equilibrium) around 240 min with the adsorption capacity of 16.1 and 25.4 mg/g for Cs and Cs/Mal-A, respectively (Fig. 7). The RY adsorption capacity of the Cs/Mal-A was 53% higher than that of the Cs membrane at equilibrium state. A little more adsorption was observed after 240 min that was not significant. At early adsorption times, the process is controlled by the rate of dye transfer from the bulk of the feed solution to the membrane surface.

The empirical kinetic data were analyzed using pseudo-first-order, pseudo-second order and modified Freundlich models (Table 5). The obtained results indicated that the pseudo-second order

Table 4. Constraints and optimal solutions of variables and response (desirability factor: 1.00)

Variables and response	Constraints			Optimal solution*
	Goal	Lower limit	Upper limit	
pH	In range	4	10	5.33
Dye initial concentration (mg/L)	In range	20	80	20.06
Dose of Cs/Mal-A membrane (g/L)	In range	0.2	1.4	1.28
RY removal efficiency (%)	Maximize	16.56	98.18	99.83

*Obtained by software

Table 5. Kinetic model parameters for the adsorption of RY on Cs/Mal-A composite

Kinetic model	Equation	Kinetic parameters				
		k_1 (1/min)	k_2 (g/mg·min)	k_f (1/g)	m -	R^2 -
Pseudo-first order	$\ln(q_e - q_t) = \ln q_e - \frac{k_1}{2.303}t$	0.023	-	-	-	0.96
Pseudo-second order	$\frac{t}{q_t} = \frac{t}{q_e} + \frac{1}{k_2 q_e^2}$	-	0.005	-	-	0.99
Modified Freundlich	$\ln q_t = \ln(k_f C_o) + \frac{1}{m}\ln t$	-	-	0.140	3.90	0.84

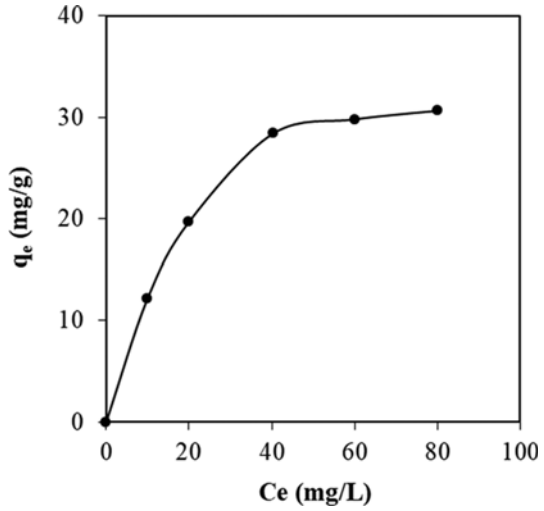

Fig. 8. Adsorption equilibrium isotherms for the Cs/Mal-A membrane at the mean level of variables ranges (agitation speed: 180 rpm, temperature: 25 °C).

equation better described the adsorption RY under experimental conditions.

The relation between the concentration of dye and the adsorption capacity of the Cs/Mal-A membrane is shown in Fig. 8. Adsorption equilibrium experiments were carried out using 0.8 g of Cs/Mal-A adsorbent in 1 L aqueous solution of RY having various initial concentrations of dye (up to 80 mg/L) at pH of 7 and 25 °C. Increasing the initial concentration of dye in the aqueous phase enhanced the adsorption capacity of the membrane. This relationship indicated that the greater the equilibrium concentration, the grater the capacity. Hereafter, because of the gradual saturation, the adsorption capacity remained unchanged, even the rise in dye concentration. The highest equilibrium capacity of 30.65 mg/L was obtained for Cs/Mal-A (0.5 wt%) composite. The Langmuir and Freundlich isotherm models were used to describe the sorption mechanism and to estimate the maximum removal efficiency on Cs/Mal-A membrane.

Table 6 presents the isotherm equation parameters for adsorption of RY on Cs/Mal-A nanocomposite. The findings indicated

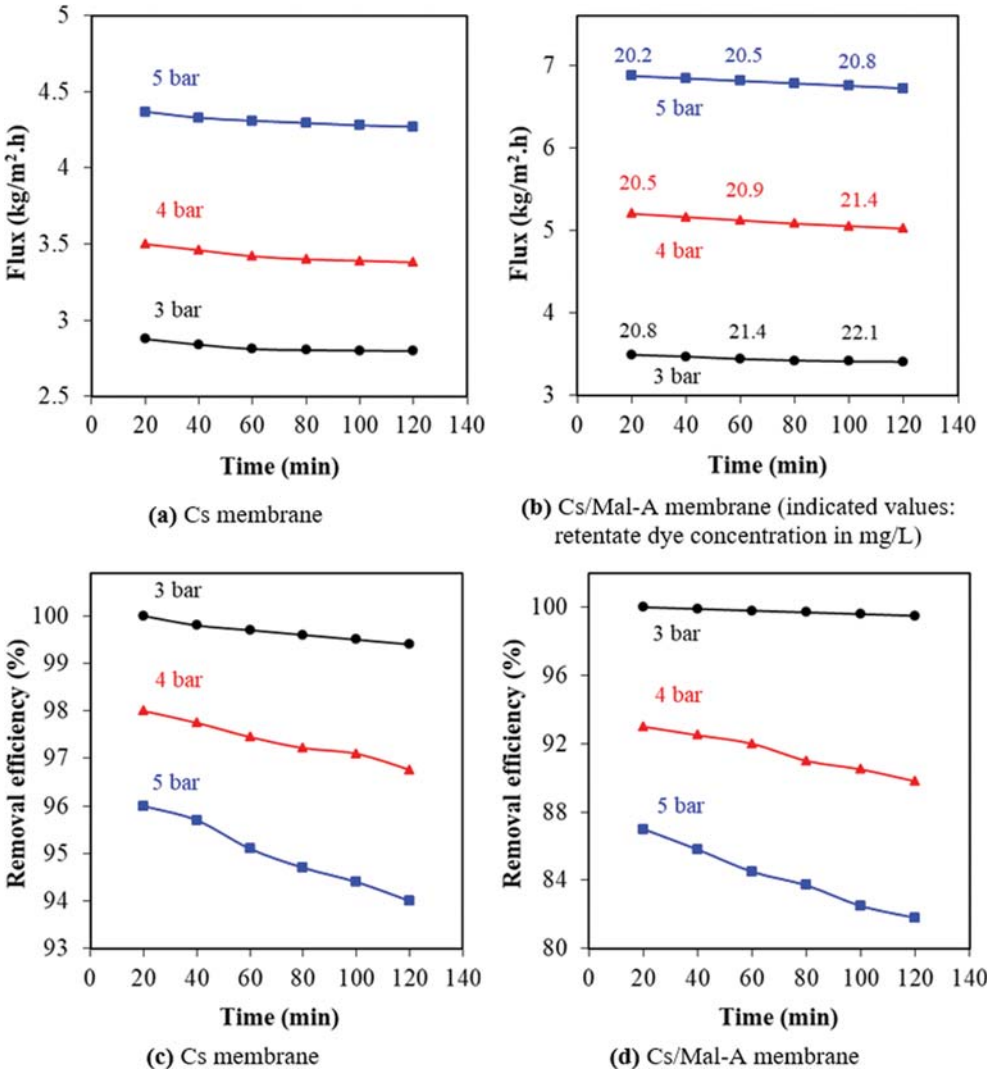

Fig. 9. Effect of trans-membrane pressure on permeate flux and removal efficiency at the optimum level of variables ranges.

Table 6. Isotherms and corresponding parameters for adsorption of RY dye on Cs/Mal-A nanocomposite

Isotherm model	Equation	q_{max} mg/g	b L/mg	K_f mg/g (L/mg)$^{1/n}$	n -	R^2 -
Langmuir	$\frac{C_e}{q_e}=\frac{1}{q_{max}b}+\frac{1}{q_{max}}C_e$	39.06	0.051	-	-	0.99
Freundlich	$\ln q_e=\ln K_f+\frac{1}{n}\ln C_e$	-	-	4.74	2.22	0.93

that the Langmuir model (R^2: 0.99) fitted the adsorption data better than the Freundlich isotherm model.

As shown in Table 6, q_{max} and b are Langmuir constants related to the maximum adsorption capacity and adsorption energy, respectively. Moreover, K_f and n are Freundlich constants related to the adsorption capacity and adsorption intensity, respectively.

6. Effect of Trans-membrane Pressure

Fig. 9(a)-(d) illustrates the permeate flux and RY removal efficiency for the Cs and Cs/Mal-A membrane that was measured under the trans-membrane pressure varying from 3 to 5 bar and for a period of 120 min. The adsorption was promoted by an electrostatic attraction between the RY molecules (with the negative charge) and the membranes (with the positive charge). As expected, an increase in hydraulic pressure across both membranes led to an increase the permeate flux; however, this was associated with a reduction in dye removal efficiency. The solute is transferred from the higher (upstream) to the lower chemical potential (downstream) through the five known consecutive steps in which the rate controlling step is diffusion across the membrane. Boundary layer effects are often overlooked. This hypothesis is most accurate when the concentration gradient is high across the membrane, and the solution is well mixed on both sides of the membrane.

In comparison with the Cs membrane, an increase in the pressure from 3 to 5 bar enhanced the permeate flux through the Cs/Mal-A membrane by 21 and 57.2% after 20 min, respectively (Fig. 9(a), (b)). At the similar period, the removal efficiency for both membranes maintained approximately 100% at 3 bar (Fig. 9(c), (d)), while the removal efficiency for Cs/Mal-A membrane decreased by 10% at 5 bar. This effect is due to the movement of ions (the H^+ ions on the surface of the Cs/Mal-A and the $-SO_3^-$ groups available in the reactive diazo dye molecules) on the membrane surface. When pressure increased, ionic crowding on the membrane surface limited the mobility of ions on the membrane surface, reducing penetration through the membrane due to formation of membrane resistance. The permeate flux was increased by approximately 96.8%, and removal efficiency was decreased by nearly 13% with increasing trans-membrane pressure of Cs/Mal-A membrane from 3 to 5 bar after 20 min. The increase in trans-membrane pressure

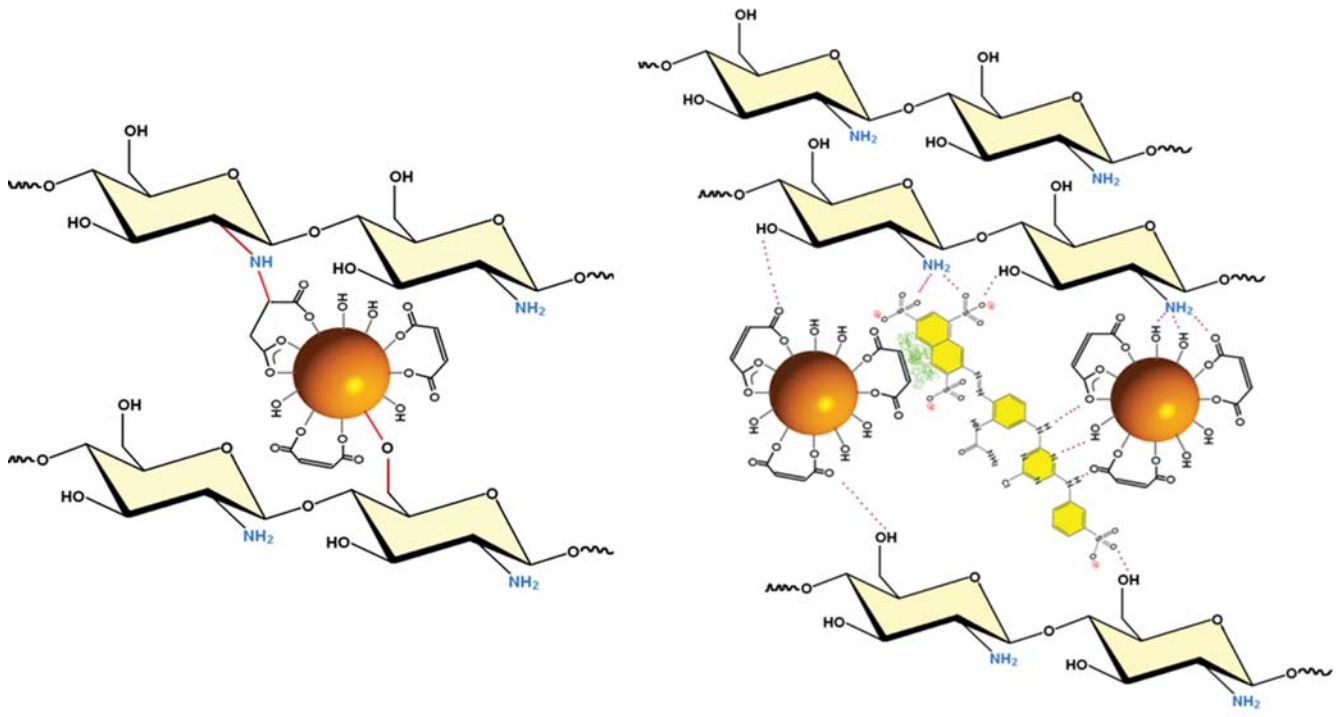

(a) Between Mal-A and Cs chains **(b)** Between Cs/Mal-A and RY dye

Fig. 10. The suggested formation of cross-linking/interaction.

increases flux in the studied pressure range (pressure control region). However, the concentration of dye on the membrane surface increases at higher pressure and the permeation flux increases gradually and is independent of pressure [37].

The effective driving force increases with pressure at a constant feed concentration and overcomes the membrane resistance [38]. Furthermore, the final retentate concentration (C_r) in the cell at 5 bar will be lower than that at 3 bar. It may be a justification for lower removal efficiency at higher pressure [39]. During the adsorption cycle, the concentration of dye was measured in retentate to study the rejection of Cs/Mal-A composite membrane (Fig. 9(b)). A slight increase in concentrations was observed for all pressure differences, indicating the presence of rejection. It decreased with pressure; however, the highest value of +1.3 mg/L (3 bar and after 120 min) did not have any major effect on membrane behavior.

The formation of cross-linking between Mal-A nanoparticles and chitosan chains is suggested in Fig. 10(a). Such interaction can be accomplished between OH groups of Mal-A nanoparticles and amine groups of chitosan chains, leading to greater tensile strength of the Cs/Mal-A membrane relative to Cs membrane. Fig. 10(b) represents the adsorption mechanism of RY on Cs and Mal-A nanoparticles in Cs/Mal-A membrane. The relatively small molecular and ionic dimension of RY 84 allows this dye to effectively penetrate the composite membrane through porous structure. Different types of interactions in the nanocomposite structure may occur among RY dye, Mal-A and chitosan molecules through the dye adsorption. It can be inferred that, a decrease in pH values and protonation of -OH and $-NH_2$ groups of Cs/Mal-A will cause increased dye adsorption. This finding was due to the increase of electrostatic bonds between $-SO_3^-$ groups of dye and the protonation of $-OH_2^+$ and $-NH_3^+$ groups of nano-particles.

More investigations are required to equate this approach with other non-adsorptive separation technologies, taking into account the trans membrane pressures obtained for the suggested membrane.

CONCLUSIONS

Maleate-Alumoxane (Mal-A) was synthesized successfully from boehmite nanoparticles and the corresponding carboxylic acid. The application of Mal-A nanoparticles to chitosan has important effects on the adsorption properties of the synthesized membranes for Reactive Yellow 84. Taking all the evidence outlined into account, the following remarks are concluded:

- The adsorption capacity of 16.1 and 25.4 mg/g was obtained for Cs and Cs/Mal-A under equilibrium condition and at the mean range of variables, respectively. The obtained results indicated an enhancement of 53% in the composite-membrane capacity due to the adsorptive properties of Mal-A structure associated with improved morphology and interconnected pores formed at 0.5 wt% of Mal-A nanoparticles in the nanocomposite membrane.

- The permeate flux was increased by nearly 96.8% and removal efficiency was decreased almost 13% with increasing trans-membrane pressure of Cs/Mal-A membrane from 3 to 5 bar after 20 min.

- The effective electrostatic forces between the RY dye molecule and the nanocomposite membrane are increased through adding Mal-A to the Cs matrix membrane.

- The results of the experimental design for RY removal by Cs/Mal-A adsorbent membrane provided appropriate quadratic model adjustment with the experimental data.

- Among the isotherms used for adsorption, the Langmuir adsorption one fitted well with the equilibrium adsorption data and the RY kinetic adsorption on Mal-A followed a pseudo-second-order kinetic model.

REFERENCES

1. N. Dow, J. V. García, L. Niadoo, N. Milne, J. Zhang, S. Gray and M. Duke, *Environ. Sci-Wat. Res.*, **3**, 433 (2017).
2. N. Barka, S. Qourzal, A. Assabbane, A. Nounah and Y. Ait-Ichou, *J. Saudi Chem. Soc.*, **15**, 263 (2011).
3. Y. Wang, T. Du, L. Zhou, Y. Song, S. Che and X. Fang, *Korean J. Chem. Eng.*, **35**, 709 (2017).
4. J. B. Parsa and F. N. Chianeh, *Korean J. Chem. Eng.*, **29**, 1585 (2012).
5. F. Li, Q. Xia, Y. Gao, Q. Cheng, L. Ding, B. Yang, Q. Tian, C. Ma, W. Sand and Y. Liu, *Environ. Sci-Wat. Res.*, **4**, 272 (2018).
6. J. Panswed and S. Wongchaisuwan, *Water Sci. Technol.*, **18**, 139 (1986).
7. C. L. Pearce, J. R. Lloyd and J. T. Guthrie, *Dyes Pigm.*, **58**, 179 (2003).
8. Y. Fu and T. Viraraghavan, *Adv. Environ. Res.*, **7**, 239 (2002).
9. N. Barka, S. Qourzal, A. Assabbane and A. Nounah, *Arab. J. Chem.*, **3**, 279 (2010).
10. R. Kant, *J. Water Resour. Prot.*, **4**, 93 (2012).
11. X. Zhu, L. Bao, Y. Wei, J. Ma and Y. Kong, *Int. J. Biol. Macromol.*, **91**, 409 (2016).
12. Z. Teimouri, A. Salem and S. Salem, *Environ. Sci. Pollut. Res.*, **26**, 7718 (2018).
13. U. Habiba, A. M. Afifi, A. Salleh and B. C. Ang, *J. Hazard. Mater.*, **322**, 182 (2017).
14. R. A. A. Muzzarelli, J. Boudrant, D. Meyer, N. Manno, M. DeMarchis and M. G. Paoletti, *Carbohydr. Polym.*, **87**, 995 (2012).
15. M. H. Dehghani, A. Dehghan, H. Alidadi, M. Dolatabadi, M. Mehrabpour and A. Converti, *Korean J. Chem. Eng.*, **34**, 1699 (2017).
16. M. Vakili, M. Rafatullah, B. Salamatinia, A. Z. Abdullah, M. H. Ibrahim, K. B. Tan, Z. Gholami and P. Amouzgar, *Carbohydr. Polym.*, **113**, 115 (2014).
17. U. Filipkowska and T. Józwiak, *J. Polym. Eng.*, **33**, 735 (2013).
18. Z. Afsarian and Y. Mansourpanah, *Korean J. Chem. Eng.*, **35**, 1867 (2018).
19. W. S. Wan Ngaha, L. C. Teong and M. A. K. M. Hanafiah, *Carbohydr. Polym.*, **83**, 1446 (2011).
20. P. Daraei, S. S. Madaeni, E. Salehi, N. Ghaemi, H. S. Ghari, M. A. Khadivi and E. Rostami, *J. Membr. Sci.*, **436**, 97 (2013).
21. A. Arafat, A. S. Sabrin, H. Dilruba, M. Mohammad and M. M. Shah, *J. Textile Sci. Eng.*, **5**, 2 (2015).
22. C. Shi, C. Lv, L. Wu and X. Hou, *J. Hazard. Mater.*, **338**, 241 (2017).
23. J. Kim and B. V. Bruggen, *Environ. Pollut.*, **158**, 2335 (2010).
24. T. A. Makhetha and R. M. Moutloali, *J. Membr. Sci.*, **554**, 195 (2018).
25. X. Zheng, X. Li, J. Li, L. Wang, W. Jin, J. Liu, Y. Pei and K. Tang, *Int. J. Biol. Macromol.*, **107**, 283 (2018).
26. R. L. Callender and A. R. Barron, *J. Mater. Res.*, **15**, 2228 (2000).
27. M. Panizza and G. Cerisola, *Water Res.*, **43**, 339 (2009).
28. J. Behin and N. Farhadian, *Appl. Water Sci.*, **7**, 3103 (2017).

29. E. Salehi, S. S. Madaeni, L. Rajabi, V. Vatanpour, A. A. Derakhshan, S. Zinadini, Sh. Ghorabi and H. Ahmadi Monfared, *Sep. Purif. Technol.*, **89**, 309 (2012).
30. A. A. Derakhshan and L. Rajabi, *Powder Technol.*, **226**, 117 (2012).
31. Z. Cheng, X. Liu, M. Han and W. Ma, *J. Hazard. Mater.*, **182**, 408 (2010).
32. A. G. Boricha and Z. V. P. Murthy, *J. Membr. Sci.*, **339**, 239 (2009).
33. T. Y. Kim and S. Y. Cho, *Korean J. Chem. Eng.*, **22**, 691 (2005).
34. Y. Mansouri, A. A. Zinatizadeh, P. Mohammadi, M. Irandoust, A. Akhbari and R. Davoodi, *Korean J. Chem. Eng.*, **29**, 891 (2012).
35. B. Krajewska, *React. Funct. Polym.*, **47**, 37 (2001).
36. S. Jana, A. Saikia, M. K. Purkait and K. Mohanty, *Chem. Eng. J.*, **170**, 209 (2011).
37. Z. F. Cui and H. S. Muralidhara, *Membrane technology*, Butterworth-Heinemann Publications, Elsevier Ltd., Burlington, USA (2010)
38. M. Syamal, S. De and P. K. Bhattacharya, *J. Membr. Sci.*, **137**, 99 (1997).
39. J. H. Huang, C. F. Zhou, G. M. Zeng, X. Li, J. Niu, H. J. Huang, L. J. Shi and S. B. He, *J. Membr. Sci.*, **365**, 138 (2010).